RSC Advances

PAPER

View Article Online
View Journal | View Issue

Cite this: *RSC Adv.*, 2015, **5**, 59003

Blocking the heat shock response and depleting HSF-1 levels through heat shock protein 90 (hsp90) inhibition: a significant advance on current hsp90 chemotherapies†

Yen Chin Koay, Jeanette R. McConnell, Yao Wang and Shelli R. McAlpine*

Clinical inhibitors of heat shock protein 90 (hsp90) modulate the N-terminus of the protein, which elicits a cell rescue cascade known as the heat shock response. This cytoprotective mechanism counteracts the impact of hsp90 chemotherapeutic agents. Inhibiting hsp90's activity *via* the C-terminus does not produce a heat shock response. Herein we report an extensive structure–activity relationship on 41 molecules that are based on the SM class of cyclic pentapeptides. This class of compounds control hsp90's C-terminus function, which induces rapid cell death without activating the heat shock response. We show that modifying single and dual side-chains was one route for producing active molecules. Moving the *N*-methyl residue around the ring also impact the biological activity of the molecule. Two of the most potent analogues were evaluated for hsp90 inhibitory activity and for their ability to reduce the heat shock response while simultaneously killing cancer cells. In addition, analysis of the most effective molecules in pharmacokinetic studies are described highlighting the compound's potential as a therapeutic drug.

Received 19th April 2015
Accepted 30th June 2015

DOI: 10.1039/c5ra07056b

www.rsc.org/advances

Introduction

Heat shock protein 90 (hsp90) has been a clinical oncogenic target since 2001.[1] Recent clinical outcomes show that molecules that modulate hsp90 *via* binding to its ATP binding site at the N-terminal domain have several drawbacks.[2] One of the most prominent issues faced by these "classical" inhibitors is the induction of a rescue cascade, which produces high levels of cytoprotective heat shock proteins (hsps), termed a heat shock response (HSR), a process governed by the transcription factor heat shock factor 1 (HSF-1). The classical hsp90 inhibitors that control hsp90's function by blocking ATP produce high levels of hsp70.[1,3–6] These hsps facilitate cancer cell survival by maintaining numerous oncogenic pathways, and promoting resistance mechanisms.[7] In contrast to these classical inhibitors, modulating hsp90's C-terminus controls its oncogenic function without inducing a HSR.[3–6] Thus, recent efforts have focused on developing new compounds that control access to hsp90's C-terminus.

Over the past several years, McAlpine and co-workers have published mechanistic data on four macrocycles, **SM122**,[3] **SM145**, **SM249** and **SM253**,[5] all of which modulate hsp90's C-terminus. These compounds block co-chaperone access to hsp90's C-terminus, inhibit numerous oncogenic pathways regulated by hsp90, and control hsp90's protein folding function, all without inducing the HSR. Indeed, this class of compound causes a significant reduction in hsp levels.[3–5]

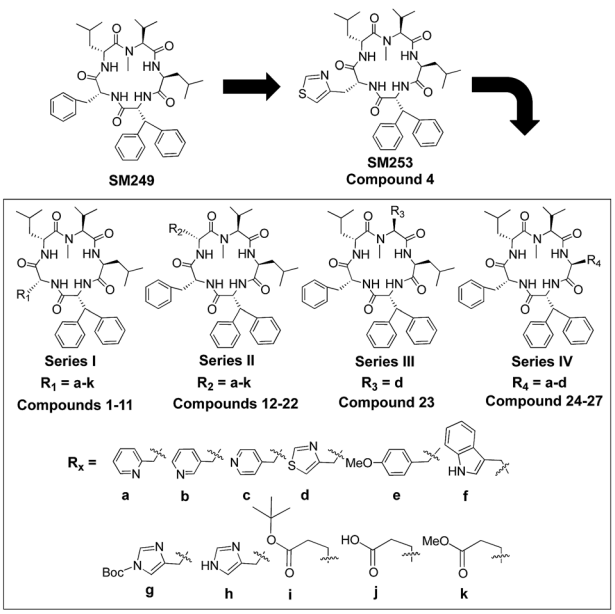

Fig. 1 Structure of analogues synthesized.

School of Chemistry, University of New South Wales, Sydney, NSW 2052, Australia. E-mail: s.mcalpine@unsw.edu.au

† Electronic supplementary information (ESI) available. See DOI: 10.1039/c5ra07056b

Herein we describe an extensive structure–activity relationship on derivatives that are based on McAlpine's most recent compounds **SM249** and **SM253** (Fig. 1). Synthesis and anticancer activity of 41 analogues in HCT116 colon cancer, and MiaPaCa-2 pancreatic cancer cell lines are described, with 35 of these compounds being reported here for the first time. The most effective analogues were then mechanistically evaluated for their ability to: (a) rapidly induce apoptosis, (b) cause phase-specific cell cycle arrest, (c) stop direct binding events between hsp90 and C-terminal co-chaperones (d) inhibit hsp90's protein folding function, and (e) reduce hsp levels associated with the HSR.

Results and discussion

Design

Our initial studies started with designing molecules based on **SM249**, which had a $GI_{50} = 7.7$ μM in HCT116, and 12.8 μM in MiaPaCa-2 cell lines. **SM249** has a $C\log P = 9.0$ (Fig. 1). Thus, the molecule was reasonably potent as a lead, but was highly insoluble. The synthesis and biological activity of series I molecules (Fig. 1), where R_1 was moiety **a–f** (*i.e.* compounds **1–6**) were recently published (Fig. 1).[5] That study produced the lead compound **SM253**, (**4**), where a thiazole moiety was placed at R_1. **SM253** had a 3 fold greater GI_{50} over **SM249**, as well as a significantly lower $C\log P$ (7.4). Thus, the incorporation of alternative moieties at R_1 was investigated. The histidine derivatives (**g** and **h**), *e.g.* compounds **7** and **8**, mimic the thiazole, while the glutamic acid derivatives (**i–k**) *e.g.* compounds **9–11**, increase the polarity of the molecule, thus improving the solubility.

Series II (Fig. 1) involved synthesizing a complete set of analogues where R_2 = **a–k**, (compounds **12–22**) thus providing the opportunity to compare activity when the same moieties were placed at different a position around the ring (Fig. 1).

Series III was only generated as a single analog, the thiazole at R_3 (Fig. 1). Finally, synthesis of molecules with moieties **a–d** were placed at position R_4 generating structures **24–27**. The biphenyl was well established to be essential to the activity of the molecule and was therefore not modified.

Synthesis

The synthesis of 35 new analogues was accomplished *via* a combination of solid phase and solution phase chemistry (Scheme 1). Analogues where positions other than R_2 were made *via* the strategy shown below, but by modifying R_1, R_3, or R_4's substituent respectively. Using a pre-loaded 2-chlorotrityl-leucine resin and then sequentially coupling fluorenylmethyloxy carbonyl (Fmoc) protected amino acids using three equivalents of coupling reagent of 1-hydroxybenzotriazole (HOBt) or 1-hydroxy-7-azabenzotriazole (HOAt) and six equivalents *N*,*N*′-diisopropylcarbodiimide (DIC) followed by deprotection of the amine led to the desired resin bound linear pentapeptide. The peptide was cleaved from the resin with 50% trifluoroethanol in dichloromethane, which generated the double de-protected linear pentapeptide, which was then cyclized using three coupling reagents 4-(4,6-dimethoxy-1,3,5-triazin-2-yl)-4-methylmorpholin-4-ium chloride (DMTMM), 2-(1*H*-7-azabenzotriazol-1-yl)-1,1,3,3-tetramethyluronium hexafluorophosphate (HATU), and *O*-(benzotriazol-1-yl)-*N*,*N*,*N*′,*N*′-tetramethyluronium tetrafluoroborate (TBTU) at 0.8 equivalent each, together with 8.0 equivalents of *N*,*N*-diisopropylethylamine (DIPEA) under dilute conditions.

N-Methylation of the individual amino acid was performed on solid supports during the linear peptide elongation. The synthesis begins with the coupling of the first amino acid on resin and, followed by the subsequent removal of the Fmoc group and the introduction of the nosyl group (2-nitrobenzenesulfonyl group), which then *N*-methylated using Mitsunobu reaction. Removal of the nosyl group is completed by nucleophilic addition reaction using 1,8-diazabicycloundec-7-ene (DBU) and 2-mercaptoethanol (Scheme 2). However, on-resin methylation on 3,3-diphenyl-D-alanine of **40** repeatedly failed, possibly because of the steric hindrance from the biphenyl ring. Thus, 3,3-diphenyl-D-alanine was methylated through nucleophilic attack of a methylation reagent, iodomethane (MeI) in the presence of a reducing agent, sodium hydride (60% dispersion in mineral oil) in anhydrous THF (0.30 M) in solution.

Structure–activity relationship study

The SAR analysis involved testing the new analogues for their cytotoxicity against HCT116 and MiaPaCa-2 cells (Table 1). The potency of these molecules was compared to the lead compound **SM253** (**4**, Table 1). This parent molecule has an GI_{50} of approximately 5 μM.[5] Of the new changes made to R_1, only the inclusion of the *tert*-butyl protected glutamic acid (**9**) improved cytotoxicity, with an GI_{50} of approximately 3 μM and 5 μM in the two cell lines respectively (Table 1). Incorporating a

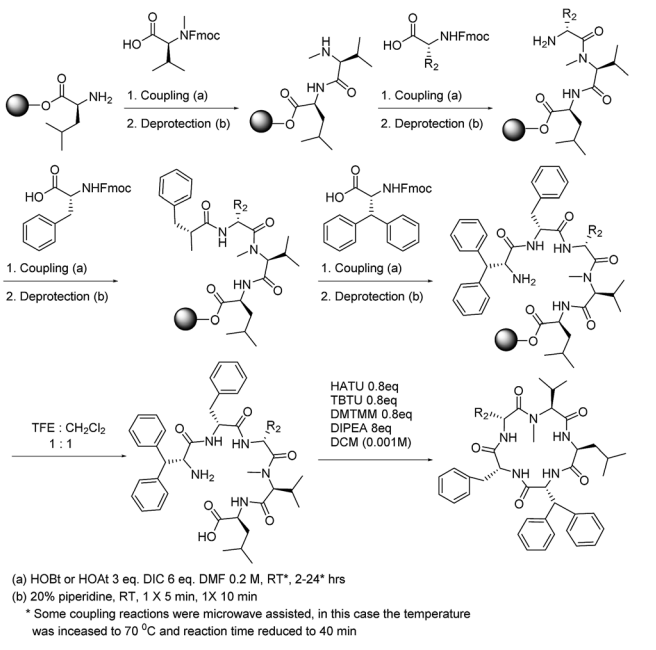

Scheme 1 General synthetic scheme of analogues.

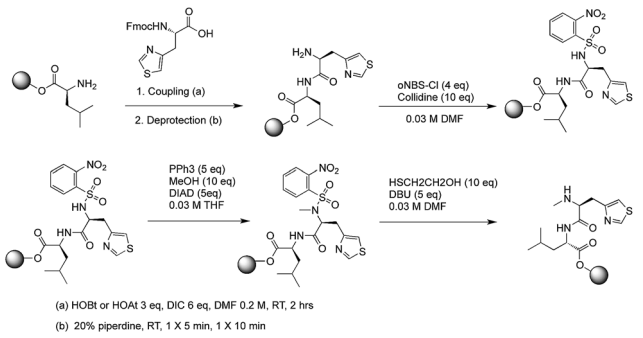

Scheme 2 Synthetic scheme to produce methylated analogues.

thiazole (**15**), methoxyphenyl (**16**), tryptophan (**17**), or a methylated glutamic acid (**22**) at R_2, improved cytotoxicity compared to **SM253**, while all the other modifications did not (Table 1).

Since the more hydrophobic nature of *t*-butyl protected glutamic acid, tryptophan, and methoxyphenyl substituents, resulting in high *C* log *P* values (8.4–9.0) and had comparable cytotoxicity to the thiazole moiety, which has a much lower *C* log *P*, we only evaluated the thiazole at position R_3, **23**. Compound **23** had a similar GI_{50} value (~6 μM) to **SM253** (Table 1). Moreover, to investigate the influence of different substituents at R_4, heterocyclic moieties **a–d** introduced at R_4 produced surprising results; the compound with a thiazole side-chain at this position (**27**) was not active, while the most

Table 1 Cytotoxicity evaluation of analogues

Cmpd #	R_x		GI_{50} (μM) HCT-116	GI_{50} (μM) MiaPaCa-2	*C* log *P*
1	R_1	**a**[a]	18.1 ± 0.4	23.6 ± 2.5	7.60
2		**b**[a]	20.8 ± 2.5	23.0 ± 2.8	7.60
3		**c**[a]	15.7 ± 2.9	18.5 ± 5.3	7.60
4 (253)		**d**[a]	5.0 ± 0.5	5.5 ± 0.2	7.44
5		**e**[a]	3.9 ± 0.2	4.5 ± 0.9	9.02
6		**f**[a]	5.1 ± 0.6	4.4 ± 0.7	9.09
7		**g**	≥30	≥30	7.91
8		**h**	≥30	≥30	6.70
9		**i**	3.0 ± 1.4	5.0 ± 1.8	8.40
10		**j**	≥30	≥30	6.79
11		**k**	9.6 ± 1.5	13.3 ± 2.1	7.17
12	R_2	**a**	≥30	≥30	7.56
13		**b**	8.8 ± 1.0	10.3 ± 0.2	7.56
14		**c**	≥30	≥30	7.56
15		**d**	3.0 ± 1.2	3.0 ± 0.8	7.40
16		**e**	5.3 ± 0.9	11.5 ± 0.5	8.98
17		**f**	6.0 ± 0.2	4.4 ± 0.9	9.05
18		**g**	≥30	≥30	7.87
19		**h**	≥30	≥30	6.66
20		**i**	≥30	≥30	8.37
21		**j**	≥30	≥30	6.75
22		**k**	5.9 ± 0.3	4.8 ± 0.6	7.13
23	R_3	**d**	6.2 ± 0.5	6.4 ± 0.6	7.93
24	R_4	**a**	6.3 ± 0.1	5.4 ± 1.0	7.56
25		**b**	15.4 ± 0.8	12.4 ± 2.0	7.56
26		**c**	22.2 ± 3.6	17.5 ± 1.8	7.56
27		**d**	≥30	≥30	7.40

[a] Indicates that structure has been reported previously.

Table 2 Cytotoxicity evaluation of dual modified analogues

Cmpd #	R_x				GI_{50} (μM) HCT-116	GI_{50} (μM) MiaPaCa-2	*C* log *P*
28	R_1	**d**	R_2	**d**	≥30	20.2 ± 4.3	5.75
29		**d**		**e**	8.4 ± 0.5	8.8 ± 0.4	7.32
30		**d**		**i**	12.4 ± 2.2	9.2 ± 1.0	6.71
31		**d**		**j**	≥30	≥30	5.10
32		**d**		**k**	≥30	≥30	5.47
33		**e**		**e**	5.2 ± 2.2	8.7 ± 1.0	8.90
34		**e**		**d**	10.4 ± 2.8	7.5 ± 0.9	7.32
35	R_1	**d**	R_4	**b**	≥30	≥30	5.91
36	R_2	**d**	R_4	**a**	19.5 ± 4.8	20.9 ± 3.8	5.87

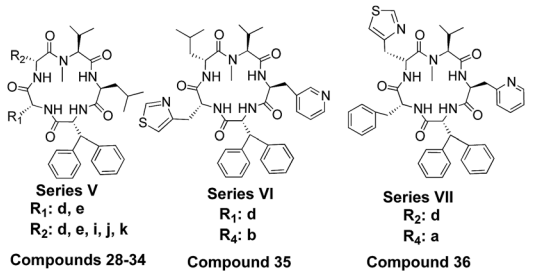

Fig. 2 Structures of dual modified analogues.

effective substitution at R_4 was the *ortho*-pyridal alanine, which had poor activity when placed at R_2 and R_3. Thus, placing a thiazole at positions R_1, R_2, and R_3 gave effective inhibitors, while a thiazole at position R_4 produced an inactive molecule.

From these series, six potent molecules were synthesized, however, these all maintained moderate cytotoxicity, with GI_{50} values of 3–6 μM. Completion of the SAR analysis using a single substitution at each position, allowed us to select the best side chains for synthesizing dual modified analogues (Table 2 and Fig. 2). Given the advantages of a thiazole moiety as a side chain, we maintained the thiazole (**d**) at R_1 and modified R_2 or R_4. Similarly, maintaining the thiazole (**d**) at R_2 we modified R_1 or R_4. The most intriguing aspect of the dual modified molecules is that all 9 compounds were less active than the lead structure, or the single modification. Thus no further analogues based on this premise were synthesized.

We[8–14] and others[15–18] have shown that placing an *N*-methyl (*N*-Me) in combination with a D-amino acid around the pentapeptide ring provides: (a) structure rigidification, which can lead to enhancing compound potency and (b) improved pharmacokinetic properties. Thus, a single analog, compound **15**, with a thiazole at R_2 was chosen as a template because it was the most potent analog with the lowest *C* log *P* to date. We performed an *N*-Me scan on compound **15** to evaluate the impact of this moiety on the biological activity. The *N*-Me substituent was rotated around this macrocycle, or removed completely, which produced a series of five additional compounds (**37–41**), (Table 3 and Fig. 3).

These methylated analogues were evaluated for their: (a) cytotoxicity, (b) the number of conformations observed on the NMR timescale (calculated from the ^{1}H NMR, Table 3). Interestingly, the

Table 3 Cytotoxicity evaluation of *N*-methylated analogues

Cmpd #	*N*-Me	GI_{50} (μM) HCT-116	GI_{50} (μM) MiaPaCa-2	*C* log *P*	# of con-formers	Ratio
15	**R_3**	**3.0 ± 1.2**	**3.0 ± 0.8**	**7.40**	**1**	**N/A**
37	R_1	24.1 ± 3.3	17.5 ± 4.2	7.40	2	70 : 30
38	R_2	14.4 ± 0.4	14.6 ± 1.2	7.40	1	N/A
39	R_4	14.9 ± 1.1	12.6 ± 2.9	7.40	1	N/A
40	R_5	18.1 ± 1.8	16.7 ± 1.5	7.40	2	69 : 31
41	N/A	8.9 ± 2.7	10.0 ± 1.7	6.75	2	80 : 20

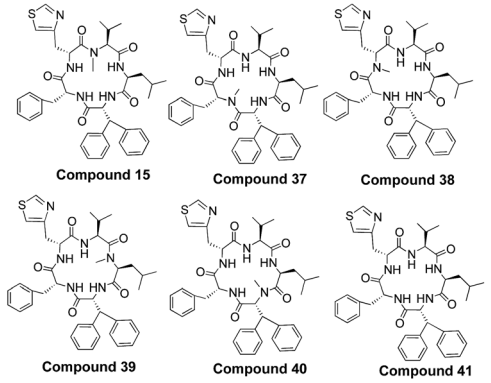

Fig. 3 Structures of *N*-methylated analogues.

lowest GI_{50} value was when an *N*-methyl was placed at R_3, *i.e.* **15**. Although compound **41** did not have an *N*-methyl moiety, it only had two conformers (previous work has shown that up to 9 conformers can exist when no *N*-Me is present in a cyclic pentapeptide). Furthermore, despite having multiple conformers, **41** was the second most potent molecule, with an $GI_{50} = \sim 9$ and ~ 10 μM respectively. The four *N*-methylated analogues, **37–40** displayed some potency but their GI_{50} values were higher than **15**. However, consistent with our data and others, compound **38** and **39**, which only had a single conformation had lower GI_{50} values than **37** and **40**, which both had 2 conformations.

Cell growth inhibition and apoptosis induction analysis

It has been established that hsp90 inhibition suppresses cancer cell growth, and eventually leads to apoptotic cell death. Thus, we evaluated and compared the ability of NVP-AUY922 and the two most active compounds, **9** and **15**, for their ability to inhibit cancer cell growth and induce apoptosis. Analysis of cell growth inhibition in HCT116 cells indicated that although at GI_{50} concentrations NVP-AUY922 showed the best inhibitory effect on cell growth, at high concentrations (5 and 10 fold over the GI_{50}), **15** was the most effective at inducing cell death (Fig. 4). NVP-AUY922 significantly reduced the percentage of cell growth to ~25% at concentrations of 5 fold over the GI_{50}; however, doubling the concentration to 10 fold GI_{50} did not improve its effectiveness. In contrast, compound **15** decreased cell growth to ~20% at 5 fold the GI_{50} concentration, and to 0% at 10 fold the GI_{50} (Fig. 4a).

Running an Annexin V/7AAD-based apoptosis assay provided important evidence on the efficiency of three inhibitors regarding their ability to induce apoptotic cancer cell death. In order to compare the their abilities in suppressing cell growth and triggering cell death, the cancer cell line, drug concentrations and the treatment time in apoptosis analysis are the same as those used in cell growth inhibition assays. Treating cells for 24 h-treatment with compound **9** at 5 and 10 fold their GI_{50} showed that the percentages of apoptotic cells in the total population were 34% and 54%, respectively (Fig. 4). By comparison, compound **15** induced extremely high levels of early and late apoptosis (Fig. 4b and c) in HCT116 cells. Indeed, 96% of cells were apoptotic after 24 h-treatment of **15** with concentration of 10 fold GI_{50} (30 μM). Interestingly, NVP-AUY922 at high concentrations (5–10 fold of its GI_{50}) failed to induce significant apoptotic cell death (Fig. 4b and c), even though it effectively inhibited cell growth (~75% inhibition, Fig. 4a) at the same concentrations. Thus, these data are highly significant as they clearly demonstrate that **15** is an extremely effective molecule for suppressing cancer cell growth by inducing apoptosis (*i.e.* it is cytotoxic). In contrast, the clinical inhibitor efficiently stops cancer cell growth, but it does not kill them, (*i.e.* it is cytostatic). Such a significant difference between **15** and NVP-AUY922 is highly supportive of our hypothesis that **15** is not inducing a HSR and the cells die immediately upon treatment, whereas NVP-AUY922 is producing a HSR, which rescues the cells. Moreover, the lack of apoptotic cell death when cells are treated with NVP-AUY922 in increasing concentrations is an indicator of perhaps why this inhibitor has done so poorly in clinical trials.

Cell cycle arrest analysis

Since hsp90 inhibition has been indicated to cause cell cycle arrest, we studied and compared the impacts of NVP-AUY922, **9** and **15** on HCT116 cell cycle distribution. Treatment of cells with NVP-AUY922 (0.05 and 0.1 μM) for 24 h produced a dose-dependent increase in the population of G0/G1 phase-cells (Fig. 5). This was accompanied by a significant reduction of cells in S and G2/M phases. Given that >75% of cells were still alive (Fig. 4b), this cell cycle data is significant and indicates that the living cells that are arrested in G0/G1 phase are likely experiencing a rescue mechanism. That is, 75% of the cells are not being triggered to die upon NVP-AUY922, rather they are being rescued by the HSR. This data also indicates that because of the activated rescue mechanism, those arrested cells were trying to fix the damage before initiating the apoptotic program. The likely rescue and damage repair scenario that is occurring

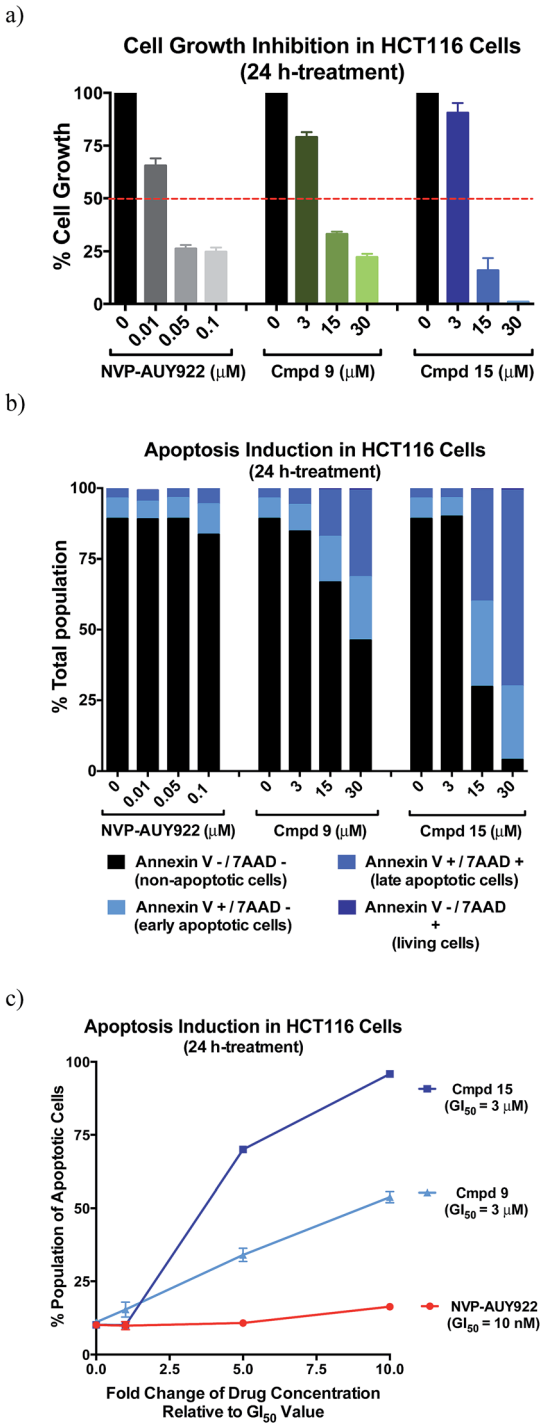

Fig. 4 (a) Cell growth inhibition activity of hsp90 inhibitors. (b) Annexin V/7AAD-based apoptosis analysis of HCT116 cells treated with hsp90 inhibitors. (c) The efficiency of hsp90 inhibitors in inducing apoptosis. All values are average ± SEM from three independent experiments.

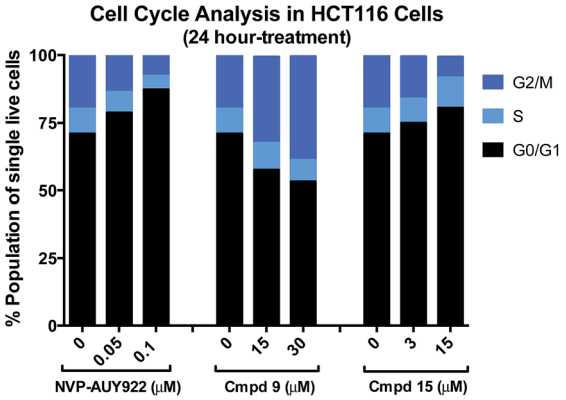

Fig. 5 The impact of hsp90 inhibitors on cell cycle distribution in HCT116 cells after 24 h.

when cells are treated with NVP-AUY922 is consistent with the observation that the compound only stopped cell growth without killing them (Fig. 4).

In comparison, after 24 h 15 μM of compound **15** also arrested cells in G0/G1 phase (Fig. 5). However, given that under the same conditions ~70% of treated cells were already apoptotic, they could not be analyzed for the cell cycle study, which only provides data on living cells. Therefore the data of compound **15** in this assay is not informative, given that it represents only 2–4% of cells. However, the cell cycle data supports the hypothesis that there is no rescue mechanism activated by **15**, which leads the treated cells to initiate apoptotic programing immediately when exposed to this compound. Interestingly, compound **9** has a distinct impact on cell cycle distribution. Even though only 50% of treated cells were still alive after the treatment with 30 μM of **9**, the cells significantly increased the population of G2/M phase-cells, and produced a corresponding sharp drop in the number of cells in G0/G1 phase (Fig. 5). This result indicates that compound **9** and **15** have distinct mechanisms that impact cancer cells. Taken together, it is clear that **15** strongly inhibits cancer cell growth as well as arresting the cell cycle arrest *via* a rapid and intensive apoptosis induction, whereas the clinical drug NVP-AUY922 does not.

Inhibitory effect on hsp90–HOP protein binding event

As a major cellular chaperone, hsp90 folds unfolded or aggregated proteins in a cell. In its protein folding mechanism, the proteins that need to be folded are transferred from hsp70 to hsp90 through the Heat shock Organizing Protein (HOP), which is a tetratricopeptide (TPR)-containing co-chaperone that interact with hsp90's C-terminus. Without the hsp90–HOP interaction, the protein-folding event is stopped, inducing a large amount of unfolded proteins accumulated inside a cell, which eventually triggers apoptotic cell death. Therefore preventing the protein-folding event by blocking the hsp90–HOP binding is a good approach to killing cancer cells.[19,20]

In order to evaluate the direct impact of compounds **9** and **15** on hsp90–HOP interaction, an *in vitro* protein-binding assay was performed by incubating native human hsp90 with different concentrations (0 up to 30 μM) of compound **9** and **15**, or NVP-AUY922, followed by the addition of His-tagged HOP and immobilizing beads. Compound **28** and NVP-AUY922 were the negative controls, as we did not expect to observe a significant effect with these compounds. The results showed that only

63% and 48% of hsp90 bound to HOP in the presence of 15 μM of compound **9** and **15**, respectively (Fig. 6). Gratifyingly, treatments with 30 μM of compound **15** efficiently blocked the binding between hsp90 and HOP by ~77%, which is ~3 fold more effective than 30 μM of compound **9** (Fig. 6).

Interestingly, NVP-AUY922, this classic inhibitor slightly disrupted the binding between HOP to hsp90 (~26%), at 0.1 μM 10-fold over NVP-AUY922's GI_{50} value. However, 10 fold over the IC_{50} compound **15** disrupted the binding by 77%, demonstrating that despite its relatively high GI_{50} against cancer cells, it effectively blocks binding to the C-terminus. These results illustrate the limitations associated with N-terminal inhibitors' hsp90 mechanism of action. Specifically they inhibit hsp90's ATPase activity, which likely plays a role in inducing the HSR, but they do not affect the binding between hsp90 and the TPR-containing protein, HOP. Thus, they cannot inhibit the protein folding or other roles regulated by HOP and hsp90. Furthermore, the data suggest that NVP-AUY922 is likely acting *via* multiple mechanisms, given that its GI_{50} = 10 nM but its IC_{50} binding affinity for hsp90 is ~5 μM. In addition, the other negative control, a structurally similar molecule **28** did not inhibit the binding event at concentration of 30 μM, which is consistent with its poor cytotoxicity in cancer cells (Fig. 5). This data clearly indicates that the binding impact is structure dependent and not a factor related to the hydrophobic impact.

Inhibitory effect on hsp90's protein folding function

In order to assess the direct inhibition of the hsp90 protein folding function by compounds **9** and **15**, we utilized the hsp90-dependent luciferase-refolding assay in rabbit reticulocyte lysate (RRL) protein-folding system. A luminescence signal is detected only if the denatured luciferase protein is refolded by hsp90 that is functionally active. On the other hand, when hsp90 is inhibited, a decreased signal will be observed. NVP-AUY922, **9**, and **15** were tested in this assay and the data is shown below (Fig. 7). Compound NVP-AUY922 only inhibits protein folding function by 5–10% at 10 fold over its IC_{50} value (Fig. 7). These data strongly indicate that infact NVP-AUY922 is not impacting any protein folding function associated with hsp90. Compound **15** is ~2 fold more effective than **9** at inhibiting hsp90's ability to refold the heat-denatured luciferase at 30 μM concentration, where **15** and **9** decreased the luciferase signal by ~70% *versus* ~35%, respectively (Fig. 7). Compound **28** was used as a negative control, and as expected, it failed to inhibit hsp90's protein folding function even at high concentrations.

As reported by others, classical inhibitors had poor inhibitory activity against the hsp90-mediated refolding of denatured luciferase. Even with concentrations of 100 fold over the GI_{50} (17-AAG at 5 μM,[21] and NVP-AUY922 at 1 μM), the classic inhibitors did not effectively inhibit the hsp90-dependent protein folding event (Fig. 7). These results clearly showed that compound **9** and **15** suppressed hsp90 protein-folding function in a concentration-dependent manner, which was more effective than the clinical candidates.

Impact on heat shock protein expression

In addition to cell growth inhibition, apoptosis induction, and the suppressive impact on hsp90–HOP protein binding and hsp90-mediated protein folding machinery, it is important to prove that the active compounds **9** and **15** do not induce the HSR as a rescue mechanism.

The HSR activation was detected by evaluating the protein expression levels of specific heat shock proteins (hsp70, hsp27, hsp90 and HSF-1) in treated HCT116 cells. Assessment of **9** and **15** for their ability to reduce hsp27, hsp70, hsp90, and HSF-1 protein levels was accomplished by treating HCT116 cells with compounds at three different concentrations. Evaluation of these 4 protein levels after 24 h indicates the activation of heat shock response: increased levels of these proteins indicate that a HSR has occurred, and the decreased levels signify the absence of a HSR.

Treating HCT116 cells with compound **9** for 24 h only reduced HSF-1 levels by a small amount (Fig. 8). However, cells treated with 30 μM of **15** eradicated the HSF-1 levels. This is unprecedented, and no drug has produced this kind of response on HSF-1. Given that HSF-1 is a key regulator of oncogenic pathways and it protects the cell, deleting this protein using a small molecule is an extremely positive outcome. In contrast, treatment with NVP-AUY922 significantly

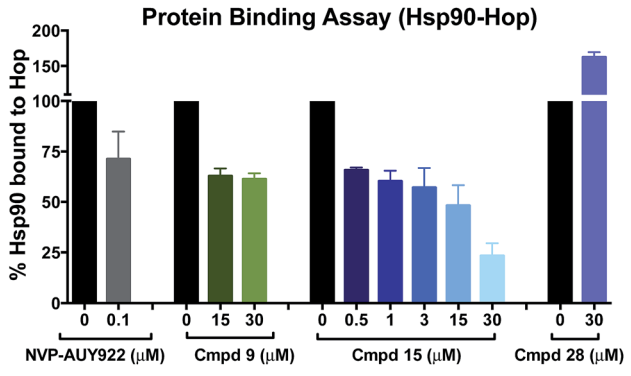

Fig. 6 The inhibitory activity of hsp90 inhibitors on the binding between hsp90 and its co-chaperone, HOP.

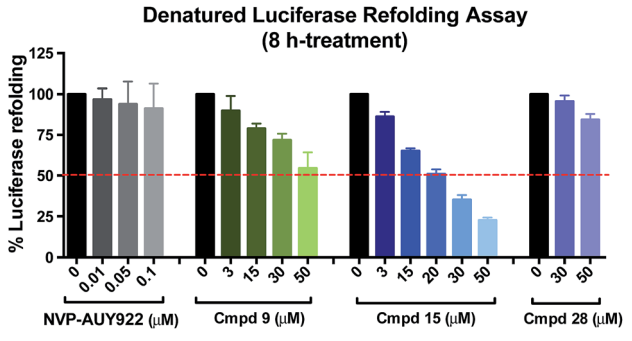

Fig. 7 The inhibitory impact of compounds on hsp90's protein folding function, which was evaluated by using the hsp90-dependent luciferase-refolding assay.

increased HSF-1 expression in a concentration-dependent manner. Specifically, at 10 fold over its GI_{50} value (100 nM) NVP-AUY922 dramatically increased HSF-1 levels by more than 10 fold.

In previous work we had shown that inhibition of hsp90 using **SM122**, **SM145**, or the clinical candidate 17-AAG (which also acts *via* the classical mechanism) does not affect hsp90 protein levels.[3–5] As seen with HCT116 cells treated with **9** (Fig. 8) does not show significant impact on hsp90 levels either. However, treating the cells with 5 fold and 10 fold over its GI_{50} value, compound **15** showed a significant decrease in hsp90 level by approximately 25% (=~1.5 fold decrease in hsp90) and 75% (=~3.0 fold decrease in hsp90), respectively. Treatment of cells with NVP-AUY922 at concentrations of 5 and 10 fold over its GI_{50} value demonstrated a slight increase in hsp90 protein levels. Thus, compound **15** is highly effective at reducing hsp90 protein levels, in contrast to the clinical candidate, which increases their levels.

Like hsp90, hsp70 expression levels were not impacted when cells were treated by compound **9** after 24 h. However, similar to **SM122** and **SM145**, treatment of **15** with 15 or 30 μM concentration reduced the amount of the cytoprotective protein hsp70 by ~2 fold and 3 fold respectively relative to the non-treated control. NVP-AUY922 treatment with concentrations of 5 and 10 fold over its GI_{50} value produced a ~4-fold increase in hsp70 protein levels (Fig. 8). These results are consistent with those published by others using NVP-AUY922, and indicate the clinical molecule is indeed producing a heat shock response.

The expression of hsp27 in HCT116 cells was effectively suppressed by treating cells with compound **9** and **15** at 30 μM (10 fold over GI_{50}), *versus* the 2.5-fold increase seen in cells treated with 100 nM of NVP-AUY922 (10 fold over GI_{50}). Since hsp27 plays an important role in the development of chemoresistance by preventing apoptosis and protein aggregation, the depletion of this protein makes our compounds highly relevant as chemotherapeutics.

In summary, **9** and **15** inhibit hsp90 activity without inducing the HSR, which makes them novel hsp90 inhibitors that overcome the resistance mechanisms associated with current and past clinical hsp90 inhibitors. Furthermore, **15** shows a unique profile that is highly advantageous as a drug treatment against cancer, in that it completely eliminates the HSF-1 levels, and strongly depletes the other two cytoprotective proteins hsp27 and hsp70.

In conclusion, we report the synthesis of 35 new compounds, including *N*-methylated derivatives. In contrast to other reports, the *N*-methyl was optimal when placed at only one position, R_3, or removed from the structure. We report here that the thiazole structure increased the molecule's potency by ~2 fold over lead **SM249** when incorporated at positions R_1–R_3, but not at R_4. Interestingly an imidazole at R_1 or R_2 completely obliterated activity, which may be due to the basicity of the imidazole moiety or the recognition of the histidine by histidases in cell leading to degradation. We also report that dual modification to molecules was less effective than a single modification. This data strongly supports our hypothesis that a specific conformation is critical for binding to hsp90 effectively.

However, without dual modifications to the macrocyclic structure, we were unable to produce highly soluble molecules and could only drop the *C* log *P* values from 9 to 7.5, which is still significantly more hydrophobic than desired. On the other hand, these molecules show a highly specific SAR, which indicates that despite their hydrophobicity they are acting *via* a defined mechanism of action. That is, if they were only cytotoxic due to their hydrophobic nature, then all compounds with similar *C* log *P* values would generate the same data. The inability of these compounds to be cytotoxic at GI_{50} levels lower than 3 μM may be related to their hydrophobicity, which limits their solubility.

The two most effective compounds, **9** and **15**, were tested in cell growth inhibition assays, apoptosis induction studies, and cell cycle distribution analysis, in order to evaluate their impact on cancer growth or death. Our data clearly indicate that as the most active compound in all those assays, **15** effectively triggers cancer cell death through a rapidly initiated apoptotic pathway, which is consistent with its strongly suppressive impact on the HSR rescue mechanism. As potential hsp90 inhibitors, the ability of **9** and **15** to inhibit hsp90 function was also well studied by: (1) detecting their effect on disrupting the interaction between hsp90 and its C-terminal co-chaperone HOP, which is a critical event in hsp90-dependent protein folding

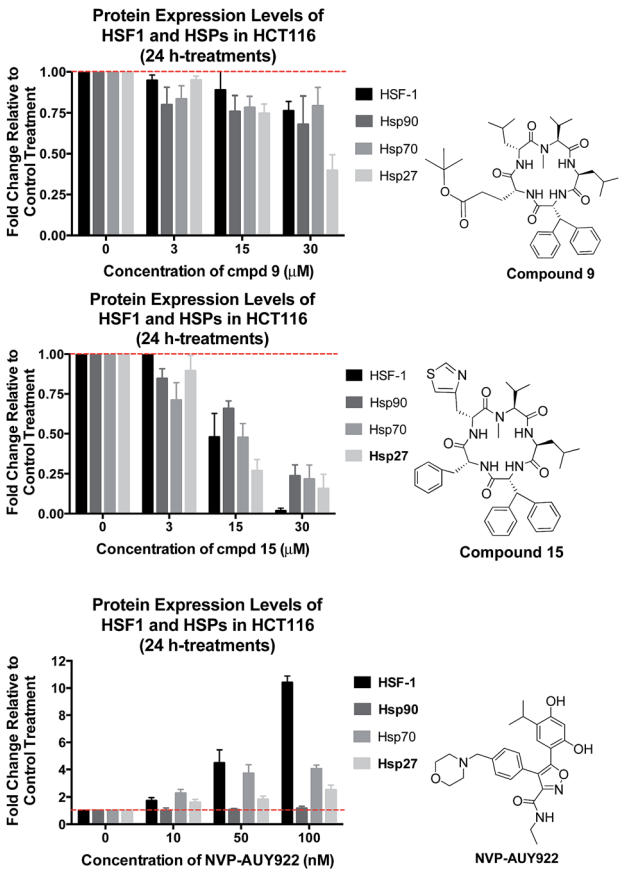

Fig. 8 The impact of hsp90 inhibitors on the heat shock response induction in HCT116 cells.

machinery, and (2) by detecting their activity in directly inhibiting hsp90's protein folding function.

Most importantly, neither compound **9** nor **15** induced the HSR rescue mechanism. Treating HCT116 cells with **9** showed a slight reduction of HSF-1, hsp90, and hsp27 protein expression levels. However, treatment of cells with **15** produced an unprecedented result: HSF-1 protein levels were completely obliterated. This has never been seen before when using an hsp90 inhibitor, where all clinical inhibitors have shown a significant increase in HSF-1 protein levels. Treatment with **15** also led to strongly decreased expression levels of hsp70 and hsp27 in cancer cells, which play critical roles in preventing apoptotic cell death. Taken all together, compound **15**, reported here the first time, exhibits extraordinary properties as an hsp90 inhibitor, behavior that will be extremely advantageous in a cancer therapy.

Experimental

General information

All moisture sensitive reactions were performed under nitrogen gas and were monitored by thin-layer chromatography (TLC) and liquid-chromatography mass spectrometry (LC/MS). TLC was performed on aluminium silica gel sheets 250 μm Whatman® (4861-820) using UV light (λ = 254 nm) as visualizing method. The developing agents for TLC include potassium permanganate (general purpose) and ninhydrin (for amine group detection). Silica gel was used for flash chromatography. LC/MS analyses were performed on a LCMS system connected to a trap running in positive electrospray ionization (ESI+) mode. The mobile phase consist of DDI water with 0.1% (v/v) formic acid (solvent A), and HPLC grade acetonitrile with 0.1% (v/v) formic acid (solvent B) at a flow rate of 0.5 mL min^{-1}, starting at 70% solvent A, 30% solvent B. The gradient elution were as follow: flow rate 2 mL min^{-1}; initial 70% solvent A, 30% solvent B hold for 35 min; at 35 min 100% solvent B hold for 18 min; at 53 min 70% solvent A, 30% solvent B hold for 7 min. ^{1}H and ^{13}C NMR spectra were obtained and recorded at 25 °C on Bruker Avance III 500 MHz and 600 MHz.

General solid phase peptide synthesis

Stepwise solid phase peptide synthesis (SPPS) was performed in a polypropylene solid-phase extraction cartridge fitted with a 20 μM polyethylene frit and pre-loaded 2-chlorotrityl resins with an approximately 0.5 mmol g^{-1} loading scale were used. The resin was weight, transferred to the cartridge and was swelled in DMF for 30 minutes prior to peptide coupling in the corresponding sequence.

Fmoc-protected amino acids coupling reaction were performed in DMF solution at 0.2 M, consisting 3.0 equiv. of amino acid, 3.0 equiv. of 1-hydroxybenzotriazole and 6.0 equiv. of diisopropylcarbodiimide. Coupling was allowed to shake for a minimum of four hours on a shaker and checked *via* ninhydrin test to confirm completion. Once completed, the coupling reaction solution was drained, and the resin was subjected to Fmoc removal. (Note: for the peptide coupling between Fmoc and *N*-methyl amino terminus, 1-hydroxybenzotriazole was replaced by 1-hydroxy-7-azabenzotriazole and the coupling process was allowed to run overnight.)

General N-terminal solid phase amine deprotection

After the peptide coupling process was completed, removal of Fmoc protecting group was performed according to the following steps: DMF wash (3 × 1 minute), 20% piperidine/DMF (1 × 5 minutes), 20% piperidine/DMF(1 × 10 minutes), DMF wash (2 × 1 minute), IPA wash (1 × 1 minute), DMF was (1 × 1 minute), IPA (1 × 1 minute), DMF (3 × 1 minute).

Cleavage of linear peptide

The eventual cleavage of linear pentapeptide from resin was carried out by swelling the resin in a mixed solution of 1 : 1 (v/v) 2,2,2-trifluoroethanol (TFE)/CH_2Cl_2 (10 millilitres per gram of dried resin) and was allow to stir for 24 hours. The suspension was then filtered through a Büchner filter, and the resin was washed repeatedly with additional CH_2Cl_2 to fully extract the cleaved peptide. The filtrate was then evaporated and dried *in vacuo* overnight. The dried solid was eventually re-dissolved in CH_2Cl_2, co-evaporated with CH_2Cl_2 several times to remove the entrapped TFE residue completely and was dried *in vacuo* overnight.

Macrocyclization procedure (syringe pump)

Macrocyclization of the double deprotected linear pentapeptide using a combination of three coupling agents (DMTMM, HATU, and TBTU) at 0.8 equivalent each, together with DIPEA (8.0 equivalents) in 75% of a calculated volume of anhydrous CH_2Cl_2 to generate a 0.001 M overall concentration. The crude and dry double deprotected linear peptide (DDLP) was dissolved in the remaining amount of CH_2Cl_2. The DDLP solution was then added to the bulk solution drop-wise using a syringe pump, over 2 hours. After the addition of all DDLP, the reaction was stirred overnight and was monitored *via* LCMS and generally complete in 1–2 hours. Upon completion, the crude product was subjected to acid–base wash to remove excess DIPEA and coupling agents. The resulting crude product was first purified by flash column chromatography, followed by reversed-phase HPLC, using a gradient of acetonitrile and deionized water with 0.1% TFA to afford the final pure compounds.

Synthesis

HO-Leu-*N*-Me-Val-D-Leu-D-Glu(O*t*Bu)-3,3-diphenyl-D-Ala-NH_2 (DDLP 9). DDL **9** was generated by using 1.00 g (0.5 mmol, 1.0 equivalent) of resin-*O*-Leu-NH_2 and the subsequent peptide coupling in the sequence as mentioned below: 0.53 g (1.5 mmol, 3.0 equivalents) of Fmoc-*N*-Me-Val-OH, 0.53 g (1.5 mmol, 3.0 equivalents) of Fmoc-D-Leu-OH, 0.64 g of Fmoc-D-Glu-γ-O*t*Bu and 0.70 g (1.5 mmol, 3.0 equivalents) of Fmoc-3,3-diphenyl-D-Ala-OH. Each peptide coupling was done in the presence of 0.20 g of HOAt (1.5 mmol, 3.0 equivalents) or 0.20 g of HOBt (1.5 mmol, 3.0 equivalents), 0.47 mL of DIC (3.0 mmol, 6.0 equivalents) and 2.5 mL of DMF to generate a concentration

of 0.20 M. The linear pentapeptide was cleaved from the resin using a mixed solution of 6 mL of TFE and 6 mL of CH_2Cl_2. The resin containing solution was filtered and dried *in vacuo* to yield the DDLP as a white solid (249 mg, overall 65%). LC/MS (ESI): *m*/*z* called for $C_{42}H_{63}N_5O_8$ (M + 1) = 766.47, found 766.45.

Macrocycle Leu-*N*-Me-Val-D-Leu-D-Glu(O*t*Bu)-3,3-Diphe-D-Ala (compound 9). Macrocycle Leu-*N*-Me-Val-D-Leu-D-Glu(O*t*Bu)-3,3-Diphe-D-Ala (compound **9**) was synthesized using 0.25 g of the DDLP generated (0.33 mmol, 1.0 equivalent), 0.08 g of TBTU (0.26 mmol, 0.80 equivalent), 0.11 g of HATU (0.29 mmol, 0.90 equivalent), 0.07 g of DMTMM (0.26 mmol, 0.80 equivalent), 0.45 mL of DIPEA (2.6 mmol, 8.0 equivalents) in anhydrous CH_2Cl_2 (326 mL, 0.001 M). The reaction was then stirred overnight and the reaction was monitored *via* LC/MS. The reaction mixture was then subjected to acid–base wash, which was extracted twice with 10% (v/v) $HCl_{(aq)}$. The organic layer was then re-extracted with a saturated of $NaHCO_3$ aqueous solution. The combined organic layers were dried over sodium sulfate, filtered, and concentrated *in vacuo*. The resulting crude product was purified *via* flash column chromatography on silica gel using an ethyl acetate–hexane gradient system, followed by purification *via* HPLC to yield compound **9** as white solid (50 mg, 21%). R_f: 0.63 (Hex : EtOAc = 0.25 : 0.75); LC/MS: *m*/*z* called for $C_{42}H_{61}N_5O_7Na_1$ (M + Na^+) = 770.45, found 770.10. HRMS (ESI-TOF): M + Na^+, found 770.4465, $C_{42}H_{61}N_5O_7Na_1$ requires 770.4469.

^{1}H NMR (600 MHz, $CDCl_3$): δ 7.90 (d, J = 9.1 Hz, NH), 7.44–7.20 (m, 10H, D-Biphe), 6.87 (br, NH), 5.28 (br, NH), 5.21 (t, J = 10.2 Hz, 1H, CHα D-Biphe), 4.96 (q, J = 7.7 Hz, 1H, CHα Val), 4.84 (d, J = 10.8 Hz, 1H CHα D-Glu), 4.62 (br, 1H, CHβ D-Biphe), 4.58 (br, NH), 3.74 (m, 2H, CHα D-Leu, CHα Leu), 3.09 (s, 3H, NCH_3), 2.37 (m, 2H, CH_2β D-Glu), 2.26 (m, 1H, CHβ Val), 2.06 (m, 1H, CH_2β D-Leu), 1.93 (br, 1H, CH_2β D-Leu), 1.71 (m, 1H, CHγ Leu), 1.62 (m, 1H, CH_2β Leu), 1.56 (m, 2H, CH_2β Leu, CH_2γ D-Glu), 1.46 (s, 9H), 1.32 (m, 1H, CH_2γ D-Glu), 1.12 (m, 1H, CHγ D-Leu), 1.00–0.76 (m, 18H, $CH_2CH(CH_3)_2$, $CHCH(CH_3)_2$).

^{13}C NMR (150 MHz, $CDCl_3$): δ 172.82, 171.86, 171.83, 171.56, 171.28, 170.01, 140.47, 140.33, 128.91, 128.80, 128.61, 128.52, 128.39, 128.32, 128.24, 127.94, 127.26, 126.99, 80.35, 63.66, 57.89, 57.35, 57.02, 54.92, 47.65, 41.96, 38.09, 31.34, 30.16, 28.12, 26.38, 25.74, 24.84, 24.82, 23.92, 22.89, 22.65, 22.19, 19.42, 18.16.

HO-Leu-*N*-Me-Val-3-(4-Thia)-D-Ala-D-Phe-3,3-Diphe-D-Ala-NH_2 (DDLP 15). DDLP **15** was generated by using 1.00 g (0.5 mmol, 1.0 equivalent) of resin-*O*-Leu-NH_2 and the subsequent peptide coupling in the sequence as mentioned below: 0.53 g (1.5 mmol, 3.0 equivalents) of Fmoc-*N*-Me-Val-OH, 0.59 g (1.5 mmol, 3.0 equivalents) of Fmoc-D-3-(4-thiazoyl)Ala-OH, 0.58 g (1.5 mmol, 3.0 equivalents) of Fmoc-D-Phe-OH and 0.70 g (1.5 mmol, 3.0 equivalents) of Fmoc-3,3-diphenyl-D-Ala-OH. Each peptide coupling was done in the presence of 0.20 g of HOAt (1.5 mmol, 3.0 equivalents) or 0.20 g of HOBt (1.5 mmol, 3.0 equivalents), 0.47 mL of DIC (3.0 mmol, 6.0 equivalents) and 2.5 mL of DMF to generate a concentration of 0.20 M. The linear pentapeptide was then cleaved from the resin using a mixed solution of 6 mL of TFE and 6 mL of CH_2Cl_2. The resin containing solution was filtered and dried *in vacuo* to yield the DDLP as a white solid (346 mg, overall 90%). LC/MS (ESI): *m*/*z* called for $C_{42}H_{52}N_6O_6S$ (M + 1) = 769.37, found 769.00.

Macrocycle Leu-*N*-Me-Val-3-(4-Thia)-D-Ala-D-Phe-3,3-Diphe-D-Ala (compound 15). Macrocycle Leu-*N*-Me-Val-3-(4-Thia)-D-Ala-D-Phe-3,3-Diphe-D-Ala (compound **15**) was synthesized using 0.35 g of the DDLP generated (0.45 mmol, 1.0 equivalent), 0.12 g of TBTU (0.36 mmol, 0.80 equivalent), 0.14 g of HATU (0.36 mmol, 0.80 equivalent), 0.10 g of DMTMM (0.36 mmol, 0.80 equivalent), 0.63 mL of DIPEA (3.6 mmol, 8.0 equivalents) in anhydrous CH_2Cl_2 (450 mL, 0.001 M). The reaction was then stirred overnight and the reaction was monitored *via* LC/MS. Upon completion, the reaction mixture was subjected to acid–base wash, which was extracted twice with 10% (v/v) $HCl_{(aq)}$. The organic layer was then re-extracted with a saturated of $NaHCO_3$ aqueous solution. The combined organic layers were dried over sodium sulfate, filtered, and concentrated *in vacuo*. The resulting crude product was purified *via* flash column chromatography on silica gel using an ethyl acetate–hexane gradient system, followed by purification *via* HPLC to yield compound **15** as white solid (151 mg, 45%). R_f: 0.39 (Hex : EtOAc = 0.25 : 0.75).

LC/MS: *m*/*z* called for $C_{42}H_{50}N_6O_5S$ (M + 1) = 751.36, found 751.05. HRMS (ESI-TOF): M + Na^+, found 773.3449, $C_{42}H_{50}N_6O_5S_1Na_1$ requires 773.3461.

^{1}H NMR (500 MHz, DMSO): δ 8.96 (d, J = 2.0 Hz, 1H, D-Thia), 8.16 (d, J = 8.6 Hz, NH), 8.08 (d, J = 8.5 Hz, NH), 7.82 (d, J = 7.5 Hz, NH), 7.55 (d, J = 9.6 Hz, NH), 7.29–7.16 (m, 15H, D-BiPhe, D-Phe), 6.87 (m, 1H, D-Thia), 5.17 (m, 1H, CHα D-BiPhe), 4.96 (q, J = 7.6 Hz, 1H, CHα D-Phe), 4.53 (d, J = 11.4 Hz, 1H, CHα Val), 4.33 (d, J = 11.8 Hz, 1H, CHβ D-BiPhe), 4.05 (m, 1H, CHα D-Thia), 3.52 (q, J = 7.5 Hz, 1H, CHα Leu), 3.29 (m, 1H, $CH_2\beta_2$ D-Phe), 2.94 (dd, J = 6.4, 14.6 Hz, 1H, $CH_2\beta_1$ D-Phe), 2.73 (dd, J = 6.9, 14.0 Hz, 1H, $CH_2\beta_2$ D-Thia), 2.64 (s, 3H, NCH_3), 2.55 (dd, J = 7.1, 14.0 Hz, 1H, $CH_2\beta_1$ D-Thia), 2.14 (m, 1H, CHβ Val), 1.48 (m, 1H, $CH_2\beta_2$ Leu), 1.38 (m, 1H, $CH_2\beta_1$ Leu), 1.21 (m, 1H, CHγ Leu), 0.81–0.61 (m, 12H, $CHCH(CH_3)_2$, $CH_2CH(CH_3)_2$).

^{13}C NMR (125 MHz, DMSO): δ 171.36, 170.34, 170.13, 169.95, 168.92, 154.04, 153.49, 141.73, 141.10, 137.54, 129.26, 129.06, 128.84, 128.74, 128.58, 128.44, 127.13, 126.93, 126.81, 115.34, 63.38, 57.22, 56.69, 53.69, 51.90, 49.90, 38.12, 37.67, 33.33, 30.30, 25.26, 24.51, 22.81, 22.58, 19.70, 18.78.

Experimental procedures and compound characterizations for compound **7–41** (excluding compound **9** and **15**) were performed as described in ESI.†

Biological methods

Cytotoxicity assay. HCT116 cells (human colorectal carcinoma) and MiaPaCa-2 cells (human pancreatic carcinoma) were obtained from ECACC. The cells were maintained in Dulbecco's Modified Eagle Medium (DMEM), supplemented with 10% fetal bovine serum (FBS) and 1% penicillin/streptomycin (Invitrogen/Life Technologies). Cells were propagated in a humidified chamber at 37 °C with 5% CO_2, seeded into 96-well plates at 2000 cells per well, and allowed to adhere overnight. The cells were then treated with varying concentrations of compounds (300 nM to 30 μM) (DMSO concentration is 1%). After 72

h-treatments the media was removed and replaced with 90 μL of DMEM and 10 μL of Cell Counting Kit 8 reagent (Dojindo) for each well. The cells were then incubated in the same chamber for another 2 hours. The absorbance for each well was read according to the manufactures protocol using a Chromate plate reader.

Luciferase refolding assay. Luciferase (Novus cat. no. NB810-74573) was diluted in stability buffer consisting of 25 mM tricine HCl (pH 7.8), 8 mM $MgSO_4$, 0.1 mM EDTA, 10% (v/v) glycerol, 1% Triton X-100, and 10 mg mL^{-1} acetylated BSA, to 100 μg mL^{-1} and denatured at 41 °C for 10 minutes. After denaturing, 10 μL of luciferase was added to 30 μL of rabbit reticulocyte lysate (Promega L4960) that had been pre-incubated at room temperature with the desired compound for 8 hours. All the compounds reported here were tested at (0, 3, 15, 20, 30, 50 μM), while the clinical hsp90 inhibitor NVP-AUY922 was tested at (0.01, 0.05, 0.1, 0.5, 1.0 μM). The luciferase was allowed to refold for 3 hour, and then 30 μL of the reaction was removed and combined with 40 μL of Bright Glo Luciferase Assay System (Promega cat. no. E2610) and read on an illuminometer (Orion). Each experiment was completed with $n = 3$.

Protein expression level analysis. HCT116 cells were seeded in 6-well plates (3×10^5 cells per well) and incubated for 24 h before treatments. Cells were treated with indicated drugs for 24 h and then lysed in lysis buffer (50 mM Tris–HCl, pH 7.4, 150 mM NaCl, 0.5% sodium deoxycholate and 0.5% NP40) supplemented with cocktail protease inhibitors (Roche) for another 24 h. The total protein concentrations of lysates were determined by the bicinchoninic acid (BCA) method with the BCA kit (Pierce) following the manufacturer's instructions. 100 μg of total protein were separated by 4–20% Tris-glycine gel (Life Technologies) and transferred to a PVDF membrane (Thermo Fisher Scientific). Membranes were blocked with 5% non-fat milk in TBST (Tris-buffered saline containing 0.1% Tween-20) for 2 h and incubated with respective primary antibodies in 2.5% non-fat milk (in TBST) at 4 °C overnight. After wash with cold TBST membranes were incubated with respective HRP-conjugated secondary antibodies at 4 °C for 2 h, following by three-time wash with cold TBST and one wash with cold TBS (Tris-buffered saline). Immunoblotting was performed using chemiluminescent substrates (Thermo scientific) and the images were captured by ImageQuant LAS 4010 digital imaging system (GE Healthcare). Each experiment was completed with $n = 3$.

Protein binding assay. The binding affinity between hsp90 and HOP completed using 200 nM (final concentration) of human native protein hsp90 and 100 nM (final concentration) of human recombinant His-tagged HOP. Experiments were carried out with concentrations ranging from 0–30 μM of compound **9** and **15**. Protein pull-down was completed using Talon-Metal Affinity Resin (Clontech, cat. no. 635501), followed by three washes of the beads in binding buffer and finally boiling the beads with 5× Laemmli sample buffer. Samples were analyzed using 4–20% SDS-PAGE gel, followed by standard Western blot protocol to detect hsp90 and HOP. The respective ratio of hsp90 to its co-chaperone or client proteins were analyzed *via* Image J and transformed to a percent of hsp90 bound to co-chaperone or client proteins. Each experiment was completed with $n = 3$.

Apoptosis and cell cycle analysis. HCT116 cells were seeded in 6-well plates with a density of 3×10^5 cells per well, incubated at 37 °C for 24 h, and then treated with indicated drugs or DMSO for another 24 h. Treated cells were harvested by trypsinization, collected and washed with phosphate buffered saline (PBS; Sigma Aldrich) for one time, and then separated equally for apoptosis and cell-cycle analyses. Cells for apoptosis analysis were stained with Annexin V-FITC (Biolegend) and 7AAD (Biolegend) in Annexin-V binding buffer (Biolegend) for 15 min, and then analyzed by using BD LSRFortessa flow cytometer immediately. Data was quantified by CellQuest software (BD Biosciences). Cells separated for cell-cycle analysis were fixed with −20 °C cold 75% ethanol (in PBS) overnight. Fixed cells were washed once with PBS and stained for 30 min with propidium iodide (PI; Life Technologies) in the presence of ribonuclease A (RNase A; Sigma Aldrich) in PBS. Cell cycle distribution was analyzed by BD LSRFortessa flow cytometer. Data was quantified by CellQuest software (BD Biosciences). All values presented are average ± SEM of at least three independent experiments.

Acknowledgements

We thank UNSW for support of S.R.M. and YCK. We also thank the Australian government for providing the Endeavour scholarship fund. Finally, we thank the NHMRC for funding (grant APP1043561).

References

1 U. Banerji, A. O'Donnell, M. Scurr, S. Pacey, S. Stapleton, Y. Asad, L. Simmons, A. Maloney, F. Raynaud, M. Campbell, M. Walton, S. Lakhani, S. Kaye, P. Workman and I. Judson, *J. Clin. Oncol.*, 2005, **23**, 4152–4161.
2 L. Whitesell and S. L. Lindquist, *Nat. Rev. Cancer*, 2005, **5**, 761–772.
3 Y. Wang and S. R. McAlpine, *Chem. Commun.*, 2015, **51**, 1410–1413.
4 J. M. McConnell, L. D. Alexander and S. R. McAlpine, *Bioorg. Med. Chem. Lett.*, 2014, **24**, 661–666.
5 Y. C. Koay, J. R. McConnell, Y. Wang, S. J. Kim and S. R. McAlpine, *ACS Med. Chem. Lett.*, 2014, **5**, 771–776.
6 V. C. Ardi, L. D. Alexander, V. A. Johnson and S. R. McAlpine, *ACS Chem. Biol.*, 2011, **6**, 1357–1367.
7 J. R. McConnell and S. R. McAlpine, *Bioorg. Med. Chem. Lett.*, 2013, **23**, 1923–1928.
8 R. P. Sellers, L. D. Alexander, V. A. Johnson, C.-C. Lin, J. Savage, R. Corral, J. Moss, T. S. Slugocki, E. K. Singh, M. R. Davis, S. Ravula, J. E. Spicer, J. L. Oelrich, A. Thornquist, C.-M. Pan and S. R. McAlpine, *Bioorg. Med. Chem.*, 2010, **18**, 6822–6856.
9 P. S. Pan, R. C. Vasko, S. A. Lapera, V. A. Johnson, R. P. Sellers, C.-C. Lin, C.-M. Pan, M. R. Davis, V. C. Ardi and S. R. McAlpine, *Bioorg. Med. Chem.*, 2009, **17**, 5806–5825.

10 K. Otrubova, G. H. Lushington, D. Vander Velde, K. L. McGuire and S. R. McAlpine, *J. Med. Chem.*, 2008, **51**, 530–544.
11 P. S. Pan, K. McGuire and S. R. McAlpine, *Bioorg. Med. Chem. Lett.*, 2007, **17**, 5072–5077.
12 K. Otrubova, K. L. McGuire and S. R. McAlpine, *J. Med. Chem.*, 2007, **50**, 1999–2002.
13 T. J. Styers, A. Kekec, R. A. Rodriguez, J. D. Brown, J. Cajica, P.-S. Pan, E. Parry, C. L. Carroll, I. Medina, R. Corral, S. Lapera, K. Otrubova, C.-M. Pan, K. L. McGuire and S. R. McAlpine, *Bioorg. Med. Chem.*, 2006, **14**, 5625–5631.
14 K. Otrubova, T. J. Styers, P.-S. Pan, R. Rodriguez, K. L. McGuire and S. R. McAlpine, *Chem. Commun.*, 2006, 1033–1034.
15 J. Chatterjee, C. Gilon, A. Hoffman and H. Kessler, *Acc. Chem. Res.*, 2008, **41**, 1331–1342.
16 C. Mas-Moruno, F. Rechenmacher and H. Kessler, *Adv. Anticancer Agents Med. Chem.*, 2010, **10**, 753–768.
17 A. C. Rand, S. S. F. Leung, H. Eng, C. J. Rotter, R. Sharma, A. S. Kalgutkar, Y. Zhang, M. V. Varma, K. A. Farley, D. B. Khunte, C. Limberakis, D. A. Price, S. Liras, A. M. Mathiowetz, M. P. Jacobsonb and R. S. Lokey, *MedChemComm*, 2012, **3**, 1282–1289.
18 J. Chatterjee, D. F. Mierke and H. Kessler, *J. Am. Chem. Soc.*, 2006, **128**, 15164–15172.
19 R. C. Vasko, R. A. Rodriguez, C. N. Cunningham, V. C. Ardi, D. A. Agard and S. R. McAlpine, *ACS Med. Chem. Lett.*, 2010, **1**, 4–8.
20 H. Wegele, S. K. Wandinger, A. B. Schmid, J. Reinstein and J. Buchner, *J. Mol. Biol.*, 2006, **356**, 802–811.
21 Y. Wang and S. R. McAlpine, *Org. Biomol. Chem.*, 2015, **13**, 2108–2116.